Impact of Scattering on the Capacity, Diversity, and Propagation Range of Multiple-Antenna Channels

Ada S. Y. Poon, *Member, IEEE*, David N. C. Tse, *Member, IEEE*, and Robert W. Brodersen, *Fellow, IEEE*

***Abstract*—The impact of scattering condition and array configuration on performances are inseparable in early analyses of multiple-antenna systems. An array-independent scattering model is introduced where three basic scattering mechanisms are modeled. Performance results become more intrinsic property of the scattering channel itself. For linear arrays of length L in an environment of total angle spread $|\Omega|$, the ergodic capacity is shown to increase linearly with $L|\Omega|$ for large arrays. When antenna arrays reduce to practical sizes, the capacity scaling depends on the signal-to-noise ratio (SNR) as well. This implies that the number of antennas used should also depend on the SNR. In terms of outage capacity, the tradeoff between spatial multiplexing gain and diversity gain is shown to be very sensitive to the underlying scattering mechanisms. Finally, as $|\Omega|$ varies with the propagation range, the tradeoff among multiplexing gain, diversity gain, and propagation range is studied.**

***Index Terms*—Antenna theory, diversity, multiple antennas, multiple-input multiple-out-put (MIMO) systems, physical channel modeling, spatial multiplexing.**

I. Introduction

MULTIPLE-antenna systems improve performance by exploiting the scattering nature of physical environments. To fully utilize this channel resource, early results [1]–[10] incorporate physical parameters of scattering condition into the channel model and study their effects on performances. They focus on models where scattering is captured by the fading statistics across all pairs of antennas. For example, [1]–[4] model the correlation across all pairs of antennas as a Kronecker product; [5]–[9] model the fading statistics as a composition of array manifolds and a random matrix capturing the scattering environment; and [10] model the fading statistics as a composition of two independent and identically distributed (i.i.d.) random matrices. While the fading statistics depends on the scattering condition, it also depends on the array configuration. As a result, different array configurations will yield different conclusions even in the *same* channel. A better understanding of the impact of scattering by itself will give us insights into choosing the array configuration and developing simpler space–time processing algorithms.

Previous work [11] proposed to capture the scattering condition by the angular intervals subtended by clusters of scatterers (see Fig. 1), and study antenna arrays that are limited by their effective aperture but not the number of antennas. Performance results therefore do not depend on the array configuration. In [11], it demonstrates that the area constraint of antenna arrays and the angular intervals subtended by scatterers put forth a deterministic limit to the number of spatial degrees of freedom. For an array of effective aperture $\mathcal{A}$ in a physical environment of total angle spread $|\Omega|$ measured in solid angle, the number of spatial degrees of freedom is shown to be $\mathcal{A}|\Omega|$ for large $\mathcal{A}$. However, knowing the angular intervals of scatterers is not enough to characterize the impact of scattering on the channel capacity and diversity gain. To carry out such analyses, the joint response between the angular intervals at the transmitter and that at the receiver needs to be modeled. The first part of this paper will supplement [11] with the joint response by modeling three basic scattering mechanisms: specular reflection, single-bounce diffuse scattering, and multibounce diffuse scattering (see Fig. 2). Based on the joint response, we will compute the channel capacity and diversity gain. Reference [12] uses a similar approach to model the antenna arrays but it uses the ray-tracing approach to model the scattering condition which lessens its analytical tractability. Our choice of the three scattering mechanisms is inspired by how they affect the path-loss exponent in the log-distance path-loss model [13]. The path-loss exponent reveals the dependence of the joint response between the transmit and the receive angular intervals: the larger the exponent is, the more diffuse the channel is, and the less dependence would be. The popular Kronecker model corresponds to the case of *no* dependence which is inconsistent with channel measurements [13] and pointed out by [14] as well.

We will first consider the fast-fading channel and compute the ergodic capacity for linear arrays of length L normalized to a wavelength

$$C = L|\Omega| \log(\gamma_1 \mathsf{SNR}) + o(L|\Omega|)$$

at high signal-to-noise ratio (SNR) where $|\Omega| := \int_\Theta \sin\theta \, d\theta$, Θ is the angular intervals subtended by scatterers, and SNR is the transmit SNR. The gain γ_1 depends on the underlying scattering mechanisms. The capacity scaling factor is $L|\Omega|$ which is consistent with the previous work on the number of degrees of freedom for large arrays [11]. When $L|\Omega|$ is only a few times of wavelength which is often the case for practical uses of multiple-

Manuscript received May 3, 2004; revised August 29, 2005. The work of A. S. Y. Poon was support by the C2S2 of the Microelectronics Advanced Research Corporation (MARCO) and DARPA.The work of D. M. C. Tse was supported in part by the National Science Foundation under Grant CCR-118784. The material in this paper was presented in part at the 36th Asilomar Conference on Signals, Systems and Computers, Pacific Grove, CA, December 2002.

A. S. Y. Poon is with the Department of Electrical and Computer Engineering, University of Illinois at Urbana-Champaign, Urbana, IL 61801 USA (e-mail: poon@uiuc.edu).

D. N. C. Tse and R. W. Brodersen are with the Department of Electrical Engineering and Computer Sciences, University of California at Berkeley, Berkeley, CA 94704 USA (e-mail: dtse@eecs.berkeley.edu; rb@eecs.berkeley.edu).

Communicated by R. R. Müller, Associate Editor for Communications.

Digital Object Identifier 10.1109/TIT.2005.864478

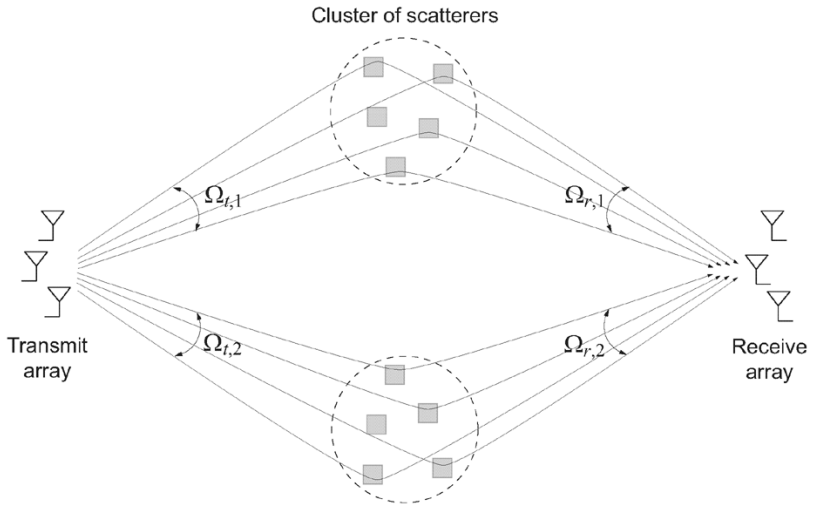

Fig. 1. Illustrates the angular interval subtended by clusters of scatterers at the transmitter $\Theta_t = \Theta_{t,1} \cup \Theta_{t,2} \cup \cdots$ and at the receiver $\Theta_r = \Theta_{r,1} \cup \Theta_{r,2} \cup \cdots$.

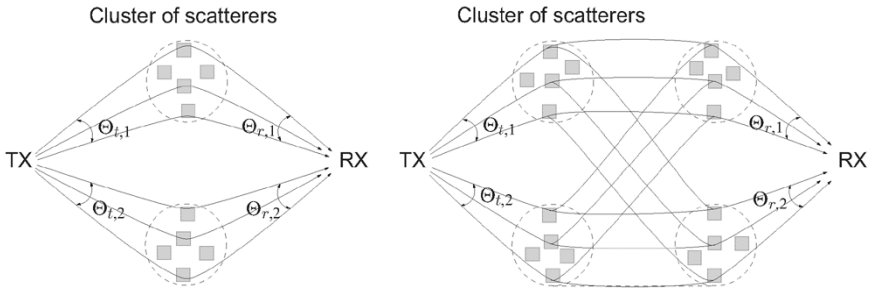

Fig. 2. Illustrates (left) single-bounce diffuse scattering and (right) multibounce diffuse scattering.

antenna systems, more terms in the capacity formula should be considered

$$C = [L|\Omega| + \gamma_2 M \ln(L|\Omega|) \ln(\gamma_1 \mathsf{SNR})] \log(\gamma_1 \mathsf{SNR}) + o(\ln(L|\Omega|)) \quad (1)$$

at high SNR where M is the number of scattering clusters. The factor γ_2 depends on the underlying scattering mechanisms. The number of spatial degrees of freedom now depends on the SNR. This phenomenon is related to the concept of super-resolution and is more relevant to the spatial domain where practical $L|\Omega|$ is not large.

For the slow-fading channel, we focus on the diversity gain and its tradeoff with the spatial multiplexing gain (data rate). The diversity gain can differ by a factor of M between single-bounce and multibounce diffuse scattering because there is more randomness in the latter than in the former. Thus, the difference between scattering mechanisms is more distinguishable in the slow fading scenario. Not only do the maximum diversity gains differ, the tradeoffs between the spatial multiplexing gain and diversity gain in the outage formulation differ as well. We will follow the tradeoff formulation in [15], and show that for a given multiplexing gain, the multibounce diffuse channel achieves an M-fold better diversity gain than the single-bounce diffuse channel in general. Since practical channels are more specular and single-bounce diffuse in nature as opposed to the Kronecker assumption, the insight obtained will help us design better space–time coding schemes.

Finally, as the scattering mechanisms studied are tied up with the path-loss model, the propagation range are therefore expected to relate to the multiplexing gain and diversity gain. We will illustrate that there is a tradeoff between propagation range and multiplexing gain. As a whole, there is a range–multiplexing–diversity tradeoff in the slow-fading channel.

The rest of the paper is organized as follows. Section II presents the scattering model. Section III computes the ergodic capacity. Section IV derives the tradeoff between multiplexing and diversity gains. Section V illustrates the tradeoff between multiplexing gain and propagation range. Finally, we will conclude this paper in Section VI.

In the following, we will use boldface capital letters for matrices and boldface lower case letter for vectors. For a vector $\boldsymbol{v}, \hat{\boldsymbol{v}}$ is a unit vector denoting its direction. $\boldsymbol{I}$ is the identity matrix. The determinant of a square matrix $\boldsymbol{A}$ is denoted by $\det(\boldsymbol{A})$ and its trace by $\mathrm{tr}(\boldsymbol{A})$. Two matrices related by $\boldsymbol{A} \succ \boldsymbol{B}$ implies that $\boldsymbol{A} - \boldsymbol{B}$ is positive definite. $\mathcal{C}^n$ and $\mathcal{C}^{n \times m}$ denote the set of n-dimensional complex vectors and $n \times m$ complex matrices, respectively. $(\cdot)^*, (\cdot)^\dagger$ and $\mathsf{E}[\cdot]$ denote the conjugate, conjugate-transpose, and expectation operations, respectively. For an uncountable set $\mathcal{S}, |\mathcal{S}|$ denotes its Lebesgue measure. $\mathcal{CN}(\mu, \sigma^2)$ denotes a complex Gaussian random variable with mean μ and variance σ^2, and $\mathcal{CN}(\boldsymbol{M}, \boldsymbol{C} \otimes \boldsymbol{D})$ denotes a complex Gaussian random matrix with mean $\boldsymbol{M}$ and covariance $\boldsymbol{C} \otimes \boldsymbol{D}$ where $\otimes$ is the Kronecker product. Two random variables related by $x \sim y$ means that they are statistically the same. $\lceil x \rceil$ gives the smallest integer equal to or greater than x.

II. Scattering Model

Following [11], we use the continuous-array model which eliminates the need to specify *a priori* the number of antennas and their relative positions. The commonly used multiple-input multiple-output (MIMO} model is a sampled version of it. Linear arrays are used to bring out the key concept. In a frequency nonselective fading channel, the transmit and the receive signals, $x(p)$ and $y(q)$, at a particular time are related by

$$y(q) = \int c(q,p)x(p)\,dp + z(q). \tag{2}$$

The channel response $c(p,q)$ gives the signal arrived at point q on the receive array due to a unit point source applied at point p on the transmit array. The additive noise $z(\cdot)$ is a white complex Gaussian random process with zero mean. The input signal is normalized such that $\mathsf{E}[\|x(p)\|^2] = \mathsf{SNR}$, the transmit SNR.

The channel response is a composition of array responses and scattering response

$$c(q,p) = \int\int a_r^*(\beta,q)h(\beta,\alpha)a_t(\alpha,p)\,d\alpha d\beta. \tag{3}$$

In the expression, the *positions p and q are normalized to a wavelength* for conciseness. In the far field, the array responses are given by

$$a_t(\alpha,p) = e^{-j2\pi\alpha p}, \qquad |p| \le \frac{L_t}{2} \tag{4a}$$

$$a_r(\beta,q) = e^{-j2\pi\beta q}, \qquad |q| \le \frac{L_r}{2} \tag{4b}$$

where $\alpha := \cos\theta$ is the directional cosine with respect to the axis of the transmit array and $\beta := \cos\vartheta$ is that with respect to the receive array (see Fig. 1). The length L_t and L_r denote the normalized length of the transmit and the receive arrays, respectively. Note that we only consider the array responses, and ignore the mutual coupling between adjacent antenna elements and between the antenna element and its surroundings. When antennas are placed closer to each other, there is mutual coupling among them that should not be ignored [16], [17]. In this case, the array response can be modeled as a product of the array response assuming no coupling and the active element response [18], [19]. The active element response then depends on the antenna spacing. To obtain a reasonable model for the active element response would require more information about the antenna type, and the dielectric properties of the antenna itself and its surroundings which is out of the scope of this paper.

The scattering response $h(\beta,\alpha)$ gives the signal received from direction β due to a unit impulse radiated to direction α. It captures the scattering condition of physical environment. As scattered paths are typically clustered around a number of disjoint angular intervals, $h(\cdot,\cdot)$ is nonzero in multiple subintervals only. With reference to Fig. 1, suppose there are M_t scattering clusters illuminated by the transmit array with angular subintervals $\Theta_{t,i}(i = 1,\ldots,M_t)$ and M_r clusters observed from the receive array with subintervals $\Theta_{r,i}(i = 1,\ldots,M_r)$. Defining $\Omega_{t,i} := \{\cos\theta : \theta \in \Theta_{t,i}\}$ and $\Omega_{r,j} := \{\cos\vartheta : \vartheta \in \Theta_{r,j}\}$, and denoting $\Omega_t := \bigcup_{i=1}^{M_t}\Omega_{t,i}$ and $\Omega_r := \bigcup_{i=1}^{M_r}\Omega_{r,i}$, the scattering response satisfies

$$h(\beta,\alpha) \neq 0 \quad \text{only if} \quad (\beta,\alpha) \in \Omega_r \times \Omega_t. \tag{5}$$

We will next model $h(\cdot,\cdot)$ within the nonzero region $\Omega_r \times \Omega_t$.

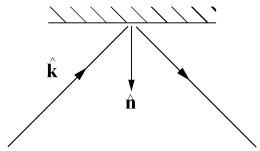

Fig. 3. Illustrates specular reflection.

Three scattering mechanisms are considered. The choice of them is inspired by how they affect the path-loss exponent in the log-distance path-loss model, a classical propagation model used to estimate the received signal strength as a function of transmit–receive separation. The path-loss exponent due to specular reflection is around 2 whereas the exponent due to diffuse scattering depends on the number of bouncing encountered by physical paths before reaching the receiver. When it is single-bounce, the exponent is around 4. In the case of multibounce, the exponent is around $2(\nu+1)$ where ν denotes the number of scattering clusters along the physical path. For example, the multibounce diffuse scattering shown in Fig. 2 has an exponent of around 6. The larger the exponent is, the more diffuse the channel is, and the less dependence in the joint response would be. Channel measurements [13] report that the path-loss exponent ranges from 2 up to 6 with typical values between 2 and 4. This implies that there is substantial dependence in the joint response. Analyses based on the Kronecker model are therefore not sufficient.

A. Specular Reflection

Starting with specular reflection, it occurs when the scattering source is smooth and large as compared to a wavelength, for example, back-wall reflection. The incident and reflected directions make equal angles from the surface normal. With reference to Fig. 3, suppose $\hat{\boldsymbol{n}}_i$ is the unit normal of the ith scattering cluster. For an impulse applied in the direction $\hat{\boldsymbol{k}} = [\sin\theta\cos\theta]^\dagger$, the signal received from the direction $\hat{\boldsymbol{\kappa}} = [\sin\vartheta\cos\vartheta]^\dagger$ is

$$e^{-j2\pi f_c\tau_i(\hat{\boldsymbol{k}})}\delta(\hat{\boldsymbol{\kappa}} - \boldsymbol{\Theta}(\hat{\boldsymbol{n}}_i)\hat{\boldsymbol{k}})\boldsymbol{\Gamma}_{SP,i}(\hat{\boldsymbol{n}}_i \times \hat{\boldsymbol{k}}, \hat{\boldsymbol{k}}) \tag{6}$$

for $\hat{\boldsymbol{k}} \in \Omega_{t,i}, i = 1,\ldots,M_t$, where f_c is the carrier frequency, $\tau_i(\hat{\boldsymbol{k}})$ is the propagation delay along $\hat{\boldsymbol{k}}$, $\boldsymbol{\Theta}(\hat{\boldsymbol{n}}_i) = \boldsymbol{I} - 2\hat{\boldsymbol{n}}_i\hat{\boldsymbol{n}}_i^\dagger$ gives the rotation on the transmit direction, and $\boldsymbol{\Gamma}_{SP,i}(\cdot,\cdot)$

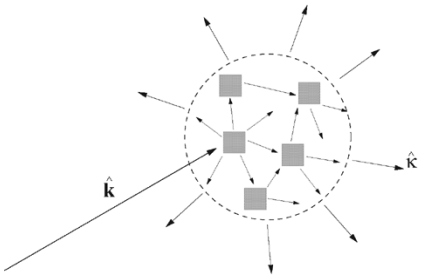

Fig. 4. Illustrates diffuse scattering from a cluster of scatterers.

denotes the change in polarization.[1] The response is inherently *deterministic*, and the transmit and receive directions are in *one-to-one correspondence*. Furthermore, as $||\boldsymbol{\Theta}(\hat{\boldsymbol{n}}_i)||$ is unity implying $|d\hat{\boldsymbol{\kappa}}| = |d\hat{\boldsymbol{k}}|$, that is, $|\Omega_{t,i}| = |\Omega_{r,i}|$, we model the specular response as

$$h_{SP}(\beta,\alpha) = e^{-j2\pi f_c \tau(\alpha)}\delta(\beta-\alpha), \quad \beta,\alpha \in \Omega_t = \Omega_r. \quad (7)$$

Note that only the measures $|\Omega_{t,i}|$ and $|\Omega_{r,i}|$ are required to be the same whereas the sets $\Omega_{t,i}$ and $\Omega_{r,i}$ need not be the same. For convenience, we assume that they are the same.

B. Diffuse Scattering

Diffuse scattering occurs when the scattering source is composed of a volume of small discrete scatterers, small as compared to a wavelength, for example, scattering by furniture. Upon impinging, the incident fields induce electric and magnetic dipoles on each discrete scatterer. The induced dipoles then *reradiate* energy to directions other than the incident direction, like a *secondary source* or *passive relay*, as shown in Fig. 4. Let us look at the response of the ith scattering cluster. Suppose $\boldsymbol{r}_n$ is the position of the nth scatterer relative to the centroid of the cluster. For an impulse applied to the direction $\hat{\boldsymbol{k}}$, the signal scattered to the direction $\hat{\boldsymbol{\kappa}}$ can be approximated by the Rayleigh scattering mechanism [20] and is

$$\frac{1}{\sqrt{N}}\sum_{n=1}^{N} e^{j\boldsymbol{k}_{e,i}^{\dagger}(\hat{\boldsymbol{\kappa}},\hat{\boldsymbol{k}})\boldsymbol{r}_n}\boldsymbol{\Gamma}_{SD,i}(\hat{\boldsymbol{\kappa}},\hat{\boldsymbol{k}}) \quad (8)$$

where $\boldsymbol{k}_{e,i}(\hat{\boldsymbol{\kappa}},\hat{\boldsymbol{k}})$ is the effective wavenumber vector of the scattering cluster along impinging direction $\hat{\boldsymbol{k}}$ and scattered direction $\hat{\boldsymbol{\kappa}}$, and $\boldsymbol{\Gamma}_{SD,i}(\cdot,\cdot)$ is the polarization matrix.[2] Compared to specular reflection, the response is inherently *stochastic*, and the transmit and receive directions are no longer in one-to-one correspondence. As the size of scattering cluster is typically large as compared to a wavelength and contains a lot of discrete scatterers, the displacement vector $\boldsymbol{r}_n$ can be modeled as a random variable in space and the phase lag $\boldsymbol{k}_{e,i}^{\dagger}(\hat{\boldsymbol{\kappa}},\hat{\boldsymbol{k}})\boldsymbol{r}_n$ is approximately uniformly distributed in $[0,2\pi)$. By the central limit theorem

$$\frac{1}{\sqrt{N}}\sum_{n=1}^{N} e^{j\boldsymbol{k}_{e,i}^{\dagger}(\hat{\boldsymbol{\kappa}},\hat{\boldsymbol{k}})\boldsymbol{r}_n} \sim \mathcal{CN}(0,1)$$

and is a function of $\hat{\boldsymbol{\kappa}}$ and $\hat{\boldsymbol{k}}$. Ignoring polarization effect, the response of a single cluster is then a complex Gaussian random process with zero mean. The second-order statistics depend on the density or roughness of the cluster as well as its dielectric properties. Without further information about the characteristics of the scattering cluster, we will model it as a white process over the angular intervals subtended by the cluster. Furthermore, we assume that clusters are uncorrelated. As a result, the single-bounce diffuse response $h_{SD}(\beta,\alpha)$ satisfies

$$\mathsf{E}[h_{SD}(\beta,\alpha)h_{SD}^{*}(\beta',\alpha')] = \delta(\beta-\beta')\delta(\alpha-\alpha'), \quad (\beta,\alpha) \in \bigcup_{i=1}^{M_t}\Omega_{r,i}\times\Omega_{t,i}. \quad (9)$$

Because of the secondary-source property of diffuse scattering, the multibounce diffuse response is a convolution of single-bounce diffuse responses. The signal radiated to $\theta \in \Theta_{t,i}(i=1,\ldots,M_t)$ is spread out and reaches the receiver from all directions over $\Theta_{r,1}\cup\cdots\cup\Theta_{r,M_r}$, as illustrated in Fig. 2(right). Now, we can model the multibounce diffuse response as $\nu-1$ convolution of independent complex Gaussian processes, each having the form of (9) where ν is the number of bouncing encountered by physical paths. But this would be difficult for closed-form analyses. To make the model more tractable while preserving the unique property of multibounce diffuse channel, we model the multibounce diffuse response $h_{MD}(\beta,\alpha)$ as a zero-mean uncorrelated complex Gaussian random process satisfying

$$\mathsf{E}[h_{MD}(\beta,\alpha)h_{MD}^{*}(\beta',\alpha')] = \frac{1}{l^{\nu-1}}\delta(\beta-\beta')\delta(\alpha-\alpha'), \quad (\beta,\alpha)\in\Omega_r\times\Omega_t \quad (10)$$

where l denotes the transmitter–receiver separation. The normalization by $l^{\nu-1}$ is due to the differential from the $\nu-1$ convolution operations.

In general, the scattering response $h(\beta,\alpha)$ is a superposition of $h_{SP}(\beta,\alpha), h_{SD}(\beta,\alpha)$, and $h_{MD}(\beta,\alpha)$. Those component responses have very different path-loss exponent. Depending on the physical environment and the carrier frequency, $h(\beta,\alpha)$ is usually dominated by one of them. Therefore, we will perform analyses on them individually.

III. Capacity

As the channel responses are continuous, we will apply a singular function expansion and result from Landau and Widom [21] on the singular value distribution to compute the capacity

[1]The polarization matrix for specular reflection is given by

$$\boldsymbol{\Gamma}_{SP,i}(\boldsymbol{v},\hat{\boldsymbol{k}}) = \frac{\eta_2\sqrt{1-v^2}-\sqrt{\eta_1^2-\eta_2^2v^2}}{\eta_2\sqrt{1-v^2}+\sqrt{\eta_1^2-\eta_2^2v^2}}\hat{\boldsymbol{v}}\hat{\boldsymbol{v}}^{\dagger} - \frac{\eta_1^2/\eta_2\sqrt{1-v^2}-\sqrt{\eta_1^2-\eta_2^2v^2}}{\eta_1^2/\eta_2\sqrt{1-v^2}+\sqrt{\eta_1^2-\eta_2^2v^2}}(\hat{\boldsymbol{v}}\times\hat{\boldsymbol{k}})(\hat{\boldsymbol{v}}\times\hat{\boldsymbol{k}})^{\dagger}$$

where v is the magnitude of $\boldsymbol{v}$, and η_1 and η_2 are the intrinsic impedance of free space and the scattering cluster respectively.

[2]The polarization matrix for diffuse scattering is given by

$$\boldsymbol{\Gamma}_{SD,i}(\hat{\boldsymbol{\kappa}},\hat{\boldsymbol{k}}) = \frac{\epsilon_r-1}{\epsilon_r+2}(\boldsymbol{I}-\hat{\boldsymbol{k}}\hat{\boldsymbol{k}}^{\dagger}) + \frac{\mu_r-1}{\mu_r+2}(\hat{\boldsymbol{\kappa}}\hat{\boldsymbol{k}}^{\dagger}-\hat{\boldsymbol{\kappa}}^{\dagger}\hat{\boldsymbol{k}}\boldsymbol{I})$$

where ϵ_r and μ_r are the relative permittivity and relative permeability of the scatterers respectively.

for the specular, multibounce diffuse, and single-bounce diffuse channels.

A. Specular Channel

In (3), the scattering response is sandwiched between two integral kernels

$$a_t(\alpha,p), \quad (\alpha,p)\in\Omega_t\times[-L_t/2,L_t/2] \tag{11a}$$
$$a_r(\beta,q), \quad (\beta,q)\in\Omega_r\times[-L_r/2,L_r/2] \tag{11b}$$

As these kernels are nonzero and square integrable, there exist two sets of orthonormal functions $\{\eta_{t,m}(\alpha)\}$ and $\{\xi_{t,m}(p)\}$, and a sequence of positive numbers in a decreasing order $\{\sigma_{t,m}\}$ such that

$$a_t(\alpha,p), \quad (\alpha,p)\in\Omega_t\times[-L_t/2,L_t/2] = \sum_{m=1}^{\infty}\sigma_{t,m}\eta_{t,m}(\alpha)\xi_{t,m}(p). \tag{12}$$

The expansion is equivalent to the singular value decomposition on finite-dimensional matrices and $\sigma_{t,m}$'s are the singular values. Similarly

$$a_r(\beta,q), \quad (\beta,q)\in\Omega_r\times[-L_r/2,L_r/2] = \sum_{n=1}^{\infty}\sigma_{r,n}\eta_{r,n}(\beta)\xi_{r,n}(q). \tag{13}$$

We project the scattering response onto the set of singular functions $\{\eta^*_{r,n}(\beta)\eta_{t,m}(\alpha)\}$, the input signal onto $\{\xi_{t,m}(p)\}$, and the output signal and additive noise onto $\{\xi_{r,n}(q)\}$. The input–output model in (2) and (3) becomes

$$y_n=\sum_{m=1}^{\infty}\sigma_{r,n}H_{nm}\sigma_{t,m}x_m+z_n, \qquad n=1,2,\ldots \tag{14}$$

For the specular channel

$$H_{nm}=\int e^{-j2\pi f_c\tau(\alpha)}\eta^*_{r,n}(\alpha)\eta_{t,m}(\alpha)\,d\alpha. \tag{15}$$

To keep up the deterministic nature of specular channel, we assume that

$$H_{nm}=e^{-j\phi_{nm}}\int\eta^*_{r,n}(\alpha)\eta_{t,m}(\alpha)\,d\alpha. \tag{16}$$

The assumption is justified for large arrays due to their good angular resolution. When $L_t=L_r$

$$H_{nm}=e^{-j\phi_{nn}}\delta_{nm} \tag{17}$$

which is diagonal. When $L_t\neq L_r$, we expect it as band diagonal. For simplicity, this paper focuses on $L_t=L_r$. The inputs and outputs in (14) are then related by

$$y_n=e^{-j\phi_{nn}}\sigma^2_{t,n}x_n+z_n, \qquad n=1,2,\ldots. \tag{18}$$

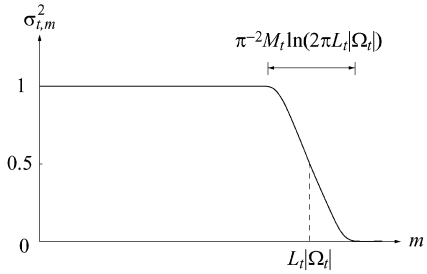

Fig. 5. Plots the distribution of $\sigma^2_{t,m}$ for large $L_t|\Omega_t|$.

The channel is composed of multiple parallel subchannels. The capacity is therefore obtained by water-filling over these subchannels and is summarized in the following lemma.

Lemma 3.1: Suppose Ω_r and Ω_t are known *a priori* at the transmitter and the receiver, respectively, $L_t=L_r$, and the receiver estimates ϕ_{nn}'s. The capacity of specular channel is

$$C_{SP}=[L_t|\Omega_t|+M_t\ln(2\pi L_t|\Omega_t|)f_1(\mathsf{SNR})]\log\left(1+\frac{\mathsf{SNR}}{L_t|\Omega_t|}\right)+o(\ln(L_t|\Omega_t|)) \tag{19}$$

as $L_t|\Omega_t|\to\infty$, where

$$f_1(\mathsf{SNR})=\frac{1}{4\pi^2}\ln\frac{\mathsf{SNR}}{L_t|\Omega_t|}+o(\ln\mathsf{SNR}) \tag{20}$$

as $\mathsf{SNR}\to\infty$.

To prove Lemma 3.1, we need to know the distribution of $\sigma^2_{t,m}$. Fortunately, Landau and Widom [21] showed that the number of $\sigma^2_{t,m}$ greater than x is given by

$$\bar{G}(x)=L_t|\Omega_t|+\frac{1}{\pi^2}M_t\ln(2\pi L_t|\Omega_t|)\ln\frac{1-x}{x}+o(\ln(L_t|\Omega_t|)) \tag{21}$$

as $L_t|\Omega_t|\to\infty$. This formula was first conjectured by Slepian in 1965 for the case when $M_t=1$ [22]. It gave a precise interpretation of the $2WT$ degrees of freedom in a class of signals that are approximately time-limited to $[-T/2,T/2]$ and frequency-limited to $[-W,W]$ in [23]. Later, in 1980, Landau and Widom proved the result for arbitrary M_t [21].

To get an idea, Fig. 5 plots the distribution of $\sigma^2_{t,m}$. There are approximately $L_t|\Omega_t|-M_t\ln(2\pi L_t|\Omega_t|)/(2\pi^2)$ number of $\sigma^2_{t,m}$'s equal to 1, and $M_t\ln(2\pi L_t|\Omega_t|)/\pi^2$ in between 0 and 1. When $L_t|\Omega_t|$ is large, those in between 0 and 1 are negligible. But when $L_t|\Omega_t|$ is not large, the fraction of $\sigma^2_{t,m}$'s in the transition region becomes significant. Based on the Landau–Widom formula, we derive the asymptotic cumulative distribution of $\sigma^2_{t,m}$. The result is summarized in the following lemma.

Lemma 3.2: Define

$$G(x):=-\frac{1}{\pi^2}M_t\ln(2\pi L_t|\Omega_t|)\ln\frac{1-x}{x} \tag{22}$$

for $0 < x < \varepsilon$, where ε satisfies

$$\ln \frac{\varepsilon}{1-\varepsilon} = -\frac{\pi^2 L_t|\Omega_t|}{M_t \ln(2\pi L_t|\Omega_t|)}. \tag{23}$$

For any increasing and bounded function $f(x)$, we have

$$\sum_{x\in\{\sigma_{t,m}^2\}, x\geq a} f(x) = \int_a^{1-\varepsilon} f(x)\, dG(x) + o(\ln(L_t|\Omega_t|)). \tag{24}$$

Now, the capacity of the specular channel can be written as

$$C_{SP} = \sum_{x\in\{\sigma_{t,m}^2\}} \log(x^2\mu)^+ \tag{25a}$$

$$= \int_{1/\sqrt{\mu}}^{1-\varepsilon} \left(\log(x^2\mu)\right)^+ dG(x) + o(\ln(L_t|\Omega_t|)) \tag{25b}$$

where μ satisfies

$$\mathsf{SNR} = \sum_{x\in\{\sigma_{t,m}^2\}} \left(\mu - \frac{1}{x^2}\right)^+ \tag{26a}$$

$$= \int \left(\mu - \frac{1}{x^2}\right)^+ dG(x) + o(\ln(L_t|\Omega_t|)) \tag{26b}$$

The rest of the proof for Lemma 3.1 is included in Appendix I.

B. Diffuse Channels

We start with the multibounce diffuse channel where we have

$$H_{nm} = \int\int \eta_{r,1}^*(\beta) h_{MD}(\beta,\alpha)\eta_{t,1}(\alpha)\, d\alpha d\beta \tag{27a}$$

$$\overset{(a)}{\sim} \frac{1}{l^{(\nu-1)/2}} \int_{\Omega_r}\int_{\Omega_t} \eta_{r,1}^*(\beta) h_w(\beta,\alpha)\eta_{t,1}(\alpha)\, d\alpha d\beta \tag{27b}$$

$$\overset{(b)}{\sim} \frac{1}{l^{(\nu-1)/2}} \int\int \eta_{r,1}^*(\beta) h_w(\beta,\alpha)\eta_{t,1}(\alpha)\, d\alpha d\beta \tag{27c}$$

$$\overset{(c)}{\sim} \frac{1}{l^{(\nu-1)/2}} \mathcal{CN}(0,1). \tag{27d}$$

The $h_w(\beta,\alpha)$ is a white complex normal process over all β and α. As $h_{MD}(\beta,\alpha)$ is a zero-mean white complex Gaussian random process over $\Omega_r \times \Omega_t$, (a) holds. The singular functions $\eta_{r,n}(\cdot)$ and $\eta_{t,m}(\cdot)$ are nonzero only over Ω_r and Ω_t, respectively, so (b) holds. The circularly symmetric property of $h_w(\beta,\alpha)$ implies (c). In conjunction with the orthonormal property of the singular functions, H_{nm}'s are independent. Apparently, the channel now becomes the standard Kronecker MIMO model. However, unlike the Kronecker model, the dimension of the fading matrix in our case is not known *a priori*. It depends on the scattering condition, array sizes, and the SNR. To compute the channel capacity, we will first derive a lower bound using tools from random matrix theory and then derive an upper bound. We will show that these bounds are asymptotically tight.

Note that the asymptotic cumulative distribution of $\sigma_{t,m}^2$ depends on $L_t|\Omega_t|$ and M_t only. That is, two channels with different Ω_t but same measure $|\Omega_t|$ and same number of disjoint subintervals M_t will yield the same performance for large L_t. For simplicity, this paper focuses on the scenario where $L_t|\Omega_t| = L_r|\Omega_r|$ and $M_t = M_r$. That is, we consider the case where the asymptotic cumulative distribution of $\sigma_{t,m}^2$ and that of $\sigma_{r,n}^2$ are approximately the same.

For any ϵ, if we consider only those $\sigma_{t,m}^2$'s greater than ϵ and pour equal power over them, this will give a lower bound. Recall that $\bar{G}(\epsilon)$ in (21) gives the number of $\sigma_{t,m}^2$ greater than ϵ. We define the empirical distribution of $\sigma_{t,m}^2$ by

$$F_\epsilon(x) := \frac{\bar{G}(\epsilon) - \bar{G}(x)}{\bar{G}(\epsilon)} \tag{28}$$

and its inverse map by $F_\epsilon^{-1}(x)$. For a fixed ϵ, as $L_t|\Omega_t|$ increases, random matrix results in Girko [24] are applied to obtain the limiting eigenvalue distribution for $l^{1-\nu}\boldsymbol{\Sigma}_\epsilon^2 \boldsymbol{H}_\epsilon \boldsymbol{\Sigma}_\epsilon^2 \boldsymbol{H}_\epsilon^\dagger$, denoted by $F_c(x)$, where $\boldsymbol{\Sigma}_\epsilon$ is a diagonal matrix of dimension $\bar{G}(\epsilon)$ with the nth diagonal element being $\sigma_{t,n}$ and $\boldsymbol{H}_\epsilon$ is a $\bar{G}(\epsilon) \times \bar{G}(\epsilon)$ matrix with the (n,m)th element being H_{nm}. Reference [3] showed that the Steltjes' transform[3] of $F_c(x)$ is given by

$$m_{F_c}(z) = \int_0^1 u(x,z)\, dx$$

and $u(x,z)$ is the unique solution to the fixed-point equation

$$u(x,z) = \left[-z + F_\epsilon^{-1}(x) \int_0^1 \frac{F_\epsilon^{-1}(p)\, dp}{1 + F_\epsilon^{-1}(p)\int_0^1 u(q,z) F_\epsilon^{-1}(q)\, dq}\right]^{-1}$$

Hence, the capacity of multibounce diffuse channel C_{MD} is lower-bounded by

$$C_{MD} \geq \bar{G}(\epsilon) \int_0^\infty \log\left(1 + \frac{\mathsf{SNR}}{l^{\nu-1}} x\right) dF_c(x). \tag{29}$$

At high SNR, it approximates

$$C_{MD} \gtrsim \bar{G}(\epsilon)\left[\log\frac{\mathsf{SNR}}{l^{\nu-1}e} + 2\int_0^1 \log F_\epsilon^{-1}(x)\, dx\right] \tag{30a}$$

$$= \bar{G}(\epsilon)\left[\log\frac{\mathsf{SNR}}{l^{\nu-1}e} + 2\int_\epsilon^1 \log x\, dF_\epsilon(x)\right]. \tag{30b}$$

The lower bound is computed and summarized in the following lemma, and the proof is included in Appendix II.

Lemma 3.3: Suppose Ω_r and Ω_t are known *a priori* at the transmitter and the receiver, respectively, $L_t|\Omega_t| = L_r|\Omega_r|, M_t = M_r$, and H_{nm}'s are known at the receiver. The ergodic capacity of the multibounce diffused channel is approximately lower-bounded by

$$C_{MD} \gtrsim [L_t|\Omega_t| + M_t \ln(2\pi L_t|\Omega_t|) f_2(\mathsf{SNR})] \log\frac{\mathsf{SNR}}{l^{\nu-1}e} + o(\ln(L_t|\Omega_t|)) \tag{31}$$

as $L_t|\Omega_t| \to \infty$, where

$$f_2(\mathsf{SNR}) = \frac{1}{4\pi^2}\ln\frac{\mathsf{SNR}}{l^{\nu-1}} + o(\ln \mathsf{SNR}) \tag{32}$$

as $\mathsf{SNR} \to \infty$.

[3]The Steltjes' transform of a distribution $F(\cdot)$ is defined by

$$m_F(z) := \int \frac{1}{x - z}\, dF(x)$$

Because $\sigma_{t,m}^2$'s are less than 1 and $\log\det$ is concave, the capacity is therefore upper-bounded by

$$C_{MD} \leq \sum_m \log\left(1+\frac{\mathsf{SNR}}{l^{\nu-1}}\sigma_{t,m}^2\right) \tag{33a}$$

$$= \int_0^{1-\varepsilon} \log\left(1+\frac{\mathsf{SNR}}{l^{\nu-1}}x\right)\, dG(x) + o(\ln(L_t|\Omega_t|)). \tag{33b}$$

It is computed in Appendix III and the result is summarized by the following lemma.

Lemma 3.4: Suppose Ω_r and Ω_t are known *a priori* at the transmitter and the receiver, respectively, $L_t|\Omega_t| = L_r|\Omega_r|, M_t = M_r$, and H_{nm}'s are known at the receiver. The ergodic capacity of the multibounce diffuse channel is upper-bounded by

$$C_{MD} \leq [L_t|\Omega_t| + M_t \ln(2\pi L_t|\Omega_t|) f_3(\mathsf{SNR})] \times \log\left(1+\frac{\mathsf{SNR}}{l^{\nu-1}}\right) + o(\ln(L_t|\Omega_t|)) \tag{34}$$

as $L_t|\Omega_t| \to \infty$, where

$$f_3(\mathsf{SNR}) = \frac{1}{2\pi^2}\ln\frac{\mathsf{SNR}}{l^{\nu-1}} + o(\ln \mathsf{SNR}) \tag{35}$$

as $\mathsf{SNR} \to \infty$.

Now, we proceed to the single-bounce diffuse channel. When L_t and L_r are large, the single-bounce channel is approximately equivalent to M_t independent single-cluster multibounce diffuse channels. Fischer's inequality assures that the optimal input covariance is separable among the M_t parallel clustered channels. Asymptotic results from multibounce diffuse channel are applied to obtain the asymptotic capacity of single-bounce diffuse channel and is summarized in Theorem 3.5.

C. Asymptotic Maximum Multiplexing Gain

Theorem 3.5: Suppose Ω_t and Ω_r are known *a priori* at the transmitter and the receiver, respectively.

- Specular channels. Assume $L_t = L_r$. The channel capacity is

$$C_{SP} = L_t|\Omega_t|\log\left(1+\frac{\mathsf{SNR}}{L_t|\Omega_t|}\right) + o(L_t|\Omega_t|) \tag{36}$$

  as $L_t|\Omega_t| \to \infty$.
- Multibounce diffuse channels. Assume $L_t|\Omega_t| = L_r|\Omega_r|$ and $M_t = M_r$. The ergodic capacity is bounded by

$$L_t|\Omega_t|\log\frac{\mathsf{SNR}}{l^{\nu-1}e} + o(L_t|\Omega_t|) \lesssim C_{MD} \leq L_t|\Omega_t|\log\left(1+\frac{\mathsf{SNR}}{l^{\nu-1}}\right) + o(L_t|\Omega_t|) \tag{37}$$

  as $L_t|\Omega_t| \to \infty$.
- Single-bounce diffuse channels. Assume

$$L_t|\Omega_{t,i}| = L_r|\Omega_{r,j}| = \frac{L_t|\Omega_t|}{M_t}, \qquad \forall i,j$$

  and M_t is finite. The ergodic capacity is bounded by

$$L_t|\Omega_t|\log\frac{\mathsf{SNR}}{M_t e} + o(L_t|\Omega_t|) \lesssim C_{SD} \leq L_t|\Omega_t|\log\left(1+\frac{\mathsf{SNR}}{M_t}\right) + o(L_t|\Omega_t|) \tag{38}$$

  as $L_t|\Omega_t| \to \infty$.

Theorem 3.5 summaries the asymptotic capacity results. All channels have the same asymptotic number of spatial degrees of freedom equal to $L_t|\Omega_t|$—the maximum spatial multiplexing gain. It is insensitive to the underlying scattering mechanisms. This result agrees with the degree-of-freedom formula in [11] where scattering mechanisms are not modeled. It supplements [11] with the capacity analysis for linear arrays. For other array geometries, the difficulty lies in finding the distribution for the singular values $\sigma_{t,m}$ and $\sigma_{r,n}$ which could be a possible extension of this work.

The underlying scattering mechanisms affect the received SNR on each spatially multiplexed channel. Several observations are worth pointing out.

- In the specular channel, as the transmit and the receive directions are in one-to-one correspondence, the received SNR per spatial channel is scaled by the number of spatial channels supported.
- In the multibounce diffuse channel, as the transmit power to a particular direction is spread out over the entire Ω_r, there is no scaling of SNR by the number of spatial channels. This phenomenon is similar to the spreading gain in waveform channels where a data symbol can be spread over multiple time-samples and/or subcarriers to increase the robustness against channel fading. In waveform channels, the spreading is done *explicitly* whereas in multiple-antenna channels, the secondary-source property of diffuse scattering brings forth the spreading *implicitly*. Also, because of the secondary-source property of diffuse scattering, a fraction of power is lost in each bouncing and therefore the received SNR is scaled by $l^{(\nu-1)}$.
- In the single-bounce diffuse channel, the transmit power emanated from $\Omega_{t,i}$ is spread over $\Omega_{r,i}$ only so the receive SNR per spatial channel is scaled by the number of clusters only.

Finally, we reiterate that the spreading benefit and path loss counteract each other in diffuse channels. Similar observation is reported in [27]. In [7], [14], channel capacities are, however, shown to be increasing with less dependence between the transmit and the receive directions, that is, multibounce diffuse channels would have better performance than specular channels. The inconsistency stems from [7], [14] keeping the receive SNR per spatial channel constant while we are keeping the total SNR constant.

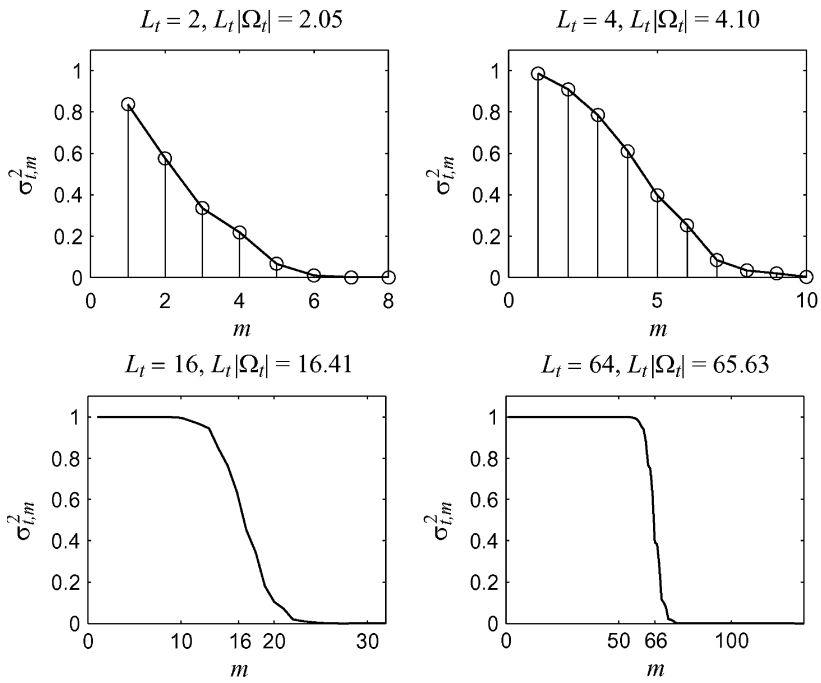

Fig. 6. Plots $\sigma^2_{t,m}$ for $\Theta_t = [25°, 55°] \cup [80°, 110°] \cup [145°, 175°]$ ($|\Omega_t| = 1.0254$) and L_t varying from 2 to 64.

D. SNR Dependence of Usable Degrees of Freedom

At high SNR, the capacity of specular channel given in Lemma 3.1 can be approximated by

$$C_{SP} \approx \left[L_t|\Omega_t| + \frac{1}{4\pi^2} M_t \ln(2\pi L_t|\Omega_t|) \ln \frac{\mathsf{SNR}}{L_t|\Omega_t|} \right] \times \log \frac{\mathsf{SNR}}{L_t|\Omega_t|} \quad (39)$$

while the capacity of the multibounce diffuse channel given in Lemmas 3.3–3.4 is approximately equal to

$$C_{MD} \approx \left[L_t|\Omega_t| + \frac{1}{c\pi^2} M_t \ln(2\pi L_t|\Omega_t|) \ln \frac{\mathsf{SNR}}{l^{\nu-1}} \right] \log \frac{\mathsf{SNR}}{l^{\nu-1}} \quad (40)$$

for some constant $c \in [2, 4]$. Apparently, there is an addition of

$$\frac{1}{4\pi^2} M_t \ln(2\pi L_t|\Omega_t|) \ln \frac{\mathsf{SNR}}{L_t|\Omega_t|}$$

degrees of freedom in the specular channel and

$$\frac{1}{c\pi^2} M_t \ln(2\pi L_t|\Omega_t|) \ln \frac{\mathsf{SNR}}{l^{\nu-1}}$$

in the multibounce diffuse channel. These additional degrees of freedom as compared to $L_t|\Omega_t|$ are negligible as $L_t|\Omega_t| \to \infty$ but become increasingly significant as $L_t|\Omega_t|$ reduces to more practical value.

The integral kernels in (11) have infinite number of nonzero singular values. In theory, if there is no noise, there will be an infinite number of degrees of freedom for information transmission. Because no matter how small the gain of a degree-of-freedom is, an infinite-precision system should be able to recover the signal carried by it. In practice, we cannot recover the signal carried by a degree-of-freedom that has gain far below the noise level. When L_t and L_r are large, the transition between good and bad singular values is so abrupt that the usable degrees of freedom is $L_t|\Omega_t|$. However, when L_t and L_r are far from infinite, the distribution of singular values is smoother. To illustrate the idea, Fig. 6 plots the distribution for different array sizes. In contrast to the discrete-array model, where the maximum spatial multiplexing gain does not depend on the SNR, the number of usable degrees-of-freedom in the continuous model depends on the noise level. That is, if we have the flexibility to place any number of antennas on the finite-array aperture, it becomes difficult to define the maximum spatial multiplexing gain. If the aperture size does not go to infinity while the SNR does, the maximum spatial multiplexing gain would be infinite. The same argument can be obtained from the concept of super-resolution [28], [29].

How can the spatial multiplexing gain go to infinity for a finite aperture? In principle, any radiating system can generate infinite number of transmission modes implying that a small array can generate the same set of transmission modes as a large array. However, in order to excite transmission modes with the same strength on both arrays, one needs to pack at least the same amount of moving charges in both arrays. More power is needed to keep the charges in the small array than in the large array.[4] Therefore, a higher SNR is required for a smaller array to have the same number of usable degrees of freedom as a larger array. When SNR goes to infinity, the number of usable degrees of freedom goes to infinity as well.

The SNR dependence implies that the number of antennas used should also depend on the SNR. To illustrate this point,

[4]Since the amount of moving charges is the same, the small array has a higher current density than the large array. A higher current density, in turn, builds up a larger radiation reaction, the self-force to hold charges together. Hence, the small array will have a poorer radiation efficiency because most of its energy is consumed to hold the charges in a small volume instead of radiating out.

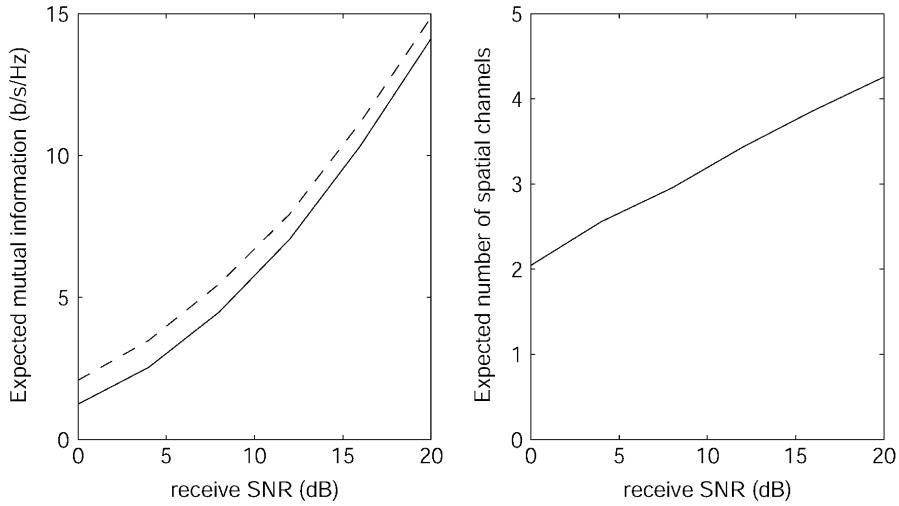

Fig. 7. Plots the expected mutual information versus the number of spatial channels at different receive SNR for $L_t = 2$. The dotted line shows the upper bound.

let us look at a numerical example. We consider a multibounce diffuse channel with three randomly placed scattering clusters each of angle 30° ($\mathsf{E}[|\Omega_t|] = \mathsf{E}[|\Omega_r|] = 1$) and array length of 2 wavelength. Water-filling is performed over singular values $\sigma_{t,m}^2$ to determine the number of spatial channels used and the amount of transmit power poured over them. The expected mutual information and the corresponding number of spatial channels for different receive SNR are plotted in Fig. 7. The upper bound shown is the ergodic capacity with full channel state information at both transmitter and receiver. The graph illustrates that the expected mutual information closely tracks the upper bound and the number of spatial channels increases with SNR. At receive SNR of 0 dB, the number of spatial channels is greater than $L_t|\Omega_t|$ on average. At receive SNR of 20 dB, the number of spatial channels is greater than $2L_t$ which corresponds to antenna spacing of less than half-wavelength.

IV. Diversity

The preceding section shows that the asymptotic ergodic capacity is insensitive to the underlying scattering mechanisms. In this section, we will show that these mechanisms have significant impact in slow-fading channels. In particular, we will illustrate how the trading between spatial multiplexing gain and diversity gain varies with the underlying scattering mechanisms. The discussion in this section will focus on the large-array regime.

Asymptotically, there are $L_t|\Omega_t|$ significant $\sigma_{t,m}^2$ and $L_r|\Omega_r|$ significant $\sigma_{r,n}^2$, and these eigenvalues are all asymptotically equal to 1. The multibounce diffuse channel is therefore approximately mimic the standard independent and identically distibuted (i.i.d.) fading model for multiple-antenna systems where the maximum diversity gain is $L_tL_r|\Omega_t||\Omega_r|$. Similarly, the single-bounce diffuse channel is approximately modeled by

$$\boldsymbol{y} = \begin{bmatrix} \boldsymbol{H}_1 & & \boldsymbol{0} \\ & \ddots & \\ \boldsymbol{0} & & \boldsymbol{H}_{M_t} \end{bmatrix} \boldsymbol{x} + \boldsymbol{z} \tag{41}$$

where $\boldsymbol{H}_i \sim \mathcal{CN}(\boldsymbol{0}, \boldsymbol{I}_{L_r|\Omega_{r,i}|} \otimes \boldsymbol{I}_{L_t|\Omega_{t,i}|})$ for $i = 1, \ldots, M_t$. The maximum diversity gain is $\sum_i L_tL_r|\Omega_{t,i}||\Omega_{r,i}|$.

Underlying scattering mechanisms not only affect the maximum diversity gain but also the tradeoff between multiplexing gain and diversity gain. To illustrate this point, we use the tradeoff formulation proposed in [15]. At a fixed target data rate, the outage probability would decay like SNR^{-d_0} at high SNR where d_0 is the maximum diversity gain. Increasing the target rate $R = r \log \mathsf{SNR}$ (bits/s/Hz), we would expect an increase in the outage probability or equivalently, the outage probability delays like $\mathsf{SNR}^{-d(r)}$ in which the exponent $d(r)$ is less than d_0 and decreases with increasing r. The curve $d(r)$ then characterizes the tradeoff between the data rate (multiplexing gain) and diversity gain. A formal definition is given below. More in-depth discussions on its operational interpretation can be found in [30, Ch. 9]. Finally, other formulations such as using the variance of mutual information [31] can also be used to illustrate such a tradeoff.

Definition 4.1: A diversity gain $d(r)$ is achieved at multiplexing gain r if the data rate is

$$R = r \log \mathsf{SNR}$$

and the outage probability is

$$P_{\text{out}}(R) \approx \mathsf{SNR}^{-d(r)}$$

or more precisely

$$\lim_{\mathsf{SNR}\to\infty} \frac{\log P_{\text{out}}(r \log \mathsf{SNR})}{\log \mathsf{SNR}} = -d(r).$$

The curve $d(r)$ characterizes the multiplexing–diversity tradeoff of the channel.

As the multibounce diffuse channel mimic the standard i.i.d. fading channel, the tradeoff curve $d_{MD}(r)$ has been solved in [15]. For the single-bounce diffuse channel, the tradeoff curve $d_{SD}(r)$ is given by solving

$$\lim_{\mathsf{SNR}\to\infty} \frac{\log P\left[\prod_{i=1}^{M_t} \det(\boldsymbol{I} + \mathsf{SNR}\boldsymbol{H}_i^\dagger \boldsymbol{H}_i) < \mathsf{SNR}^r\right]}{\log \mathsf{SNR}} = -d_{SD}(r). \tag{42}$$

The curve is computed in Appendix IV and is summarized in Theorem 4.2.

Theorem 4.2: Suppose Ω_t and Ω_r are known *a priori* at the transmitter and the receiver, respectively, and H_{nm}'s are known at the receiver. Denote the maximum multiplexing gain as

$$r_0 := \min\{L_t|\Omega_t|, L_r|\Omega_r|\}.$$

- Multibounce diffuse channels. The tradeoff curve is given by a piecewise-linear function connecting the points $(r, d_{MD}(r)), r = 0, \ldots, r_0$, where
$$d_{MD}(r) = (L_t|\Omega_t| - r)(L_r|\Omega_r| - r) \tag{43}$$
- Single-bounce diffuse channels. The tradeoff curve is
$$d_{SD}(r) = d_1(r) \oplus d_2(r) \oplus \cdots \oplus d_{M_t}(r) \tag{44}$$
where $d_i(r)$ is a piecewise-linear function connecting the points $(r, d_i(r)), r = 0, \ldots, \min\{L_t|\Omega_{t,i}|, L_r|\Omega_{r,i}|\}$ and
$$d_i(r) = (L_t|\Omega_{t,i}| - r)(L_r|\Omega_{r,i}| - r) \tag{45}$$
The operation $\oplus$ denotes the min-plus convolution and is defined as
$$(f \oplus g)(t) = \inf_{0 \le s \le t}\{f(t-s) + g(s)\}. \tag{46}$$
Descriptively, the tradeoff curve is obtained by putting end-to-end the different linear pieces in $d_i(r)$'s, sorted by increasing slopes (o,r equivalently, decreasing negative slopes).

To get an idea on the differences in the tradeoff, let us consider the scenario where the number of disjoint subintervals in Ω_t and Ω_r are equal, and the respective subintervals are of equal length. Then, $d_{SD}(r)$ is the piecewise-linear function connecting the points $(m, d_{SD}(r)), r = 0, M_t, \ldots, r_0$, where

$$d_{SD}(r) = \frac{1}{M_t}(L_t|\Omega_t| - r)(L_r|\Omega_r| - r). \tag{47}$$

Compared to $d_{MD}(r)$ in (43), the multibounce channel achieves an M_t-fold better diversity gain than the single-bounce channel in supporting a multiplexing gain which is a multiple of M_t. Fig. 8. plots the two curves for $r_0 = 4$ and $M_t = 2$.

Recent space–time code design mainly focuses on the i.i.d. fading channel (equivalent to the multibounce diffuse channel). However, real channels are more specular and single-bounce diffuse in nature. Understanding the differences on the tradeoff sheds light on designing more efficient space–time coding schemes that can adapt to the physical environment. Imagining, if we design a space–time code that is optimal for the i.i.d. fading channel and use it in a single-bounce diffuse channel, the link reliability can be much worse.

Finally, it is possible to turn a single-bounce diffuse channel into a multibounce diffuse channel by increasing the antenna spacing. This plausibly increases the diversity gain and validate the performance analyses based on the i.i.d. fading model. However, when the array length is fixed, using less antennas decreases the spatial degrees of freedom. The resulting tradeoff curve remains upper-bounded by the curve given in Theorem 4.2.

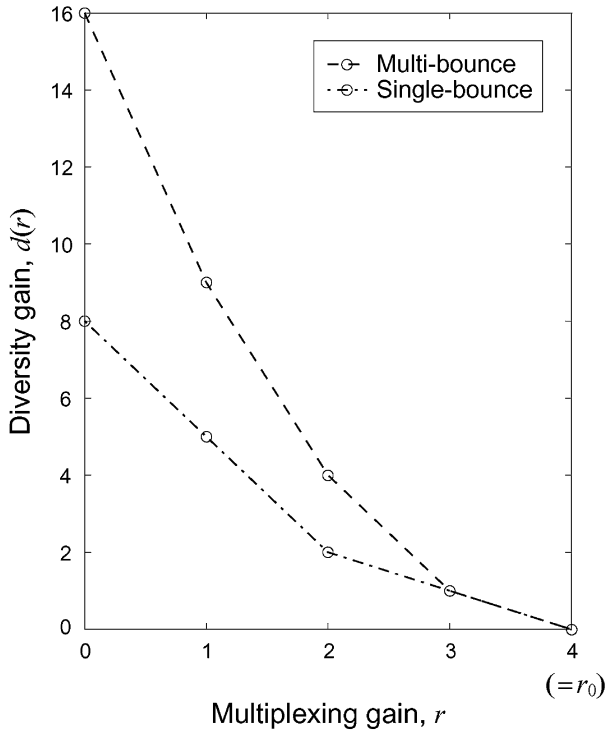

Fig. 8. Contrasts the multiplexing–diversity tradeoff curves for the multibounce and the single-bounce diffuse channels where $M_t = M_r = 2, L_t|\Omega_{t,i}| = 2$, and $L_r|\Omega_{r,i}| = 2$ for $i = 1, 2$.

V. Propagation Range

As the scattering mechanisms are tied up with the path-loss model, the propagation range is therefore related to the multiplexing gain and diversity gain. For example, [27] points out the tradeoff between path-loss and multiplexing gain across different scattering mechanisms: specular reflection has better path-loss but worse multiplexing gain whereas diffuse scattering has worse path-loss but better multiplexing gain. Under the *same* scattering mechanism, we will illustrate that there is also a tradeoff between propagation range and multiplexing gain. The analysis involved is not as vigorous as that in previous sections on ergodic capacity and diversity gain. At the least, it gives us a more comprehensive perspective on the range–multiplexing–diversity tradeoff.

If the scattering clusters remain fixed while the transmitter–receiver separation is changing, we would expect

$$|\Omega_t|, |\Omega_r| \propto \frac{1}{l}. \tag{48}$$

Recall that l is the propagation range. As the asymptotic multiplexing gain is proportional to $|\Omega_t|, |\Omega_r|$, there exists a tradeoff between multiplexing gain and propagation range under the same scattering mechanism. However, in general, changing the transmitter–receiver separation will bring in or fade out scattering clusters. For example, Fig. 9 shows a physical environment where scattering clusters are located midway between the transmitter and the receiver. When the transmitter and receiver are farther apart, there are apparently more clusters visible by them. On the other hand, when they are closer, there

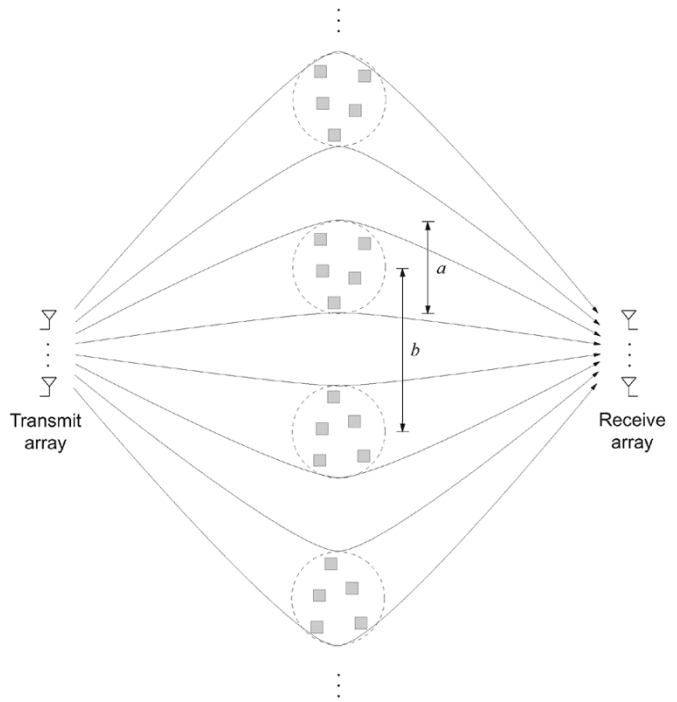

Fig. 9. A physical environment with an infinite line of scattering clusters in the midway between transmitter and receiver.

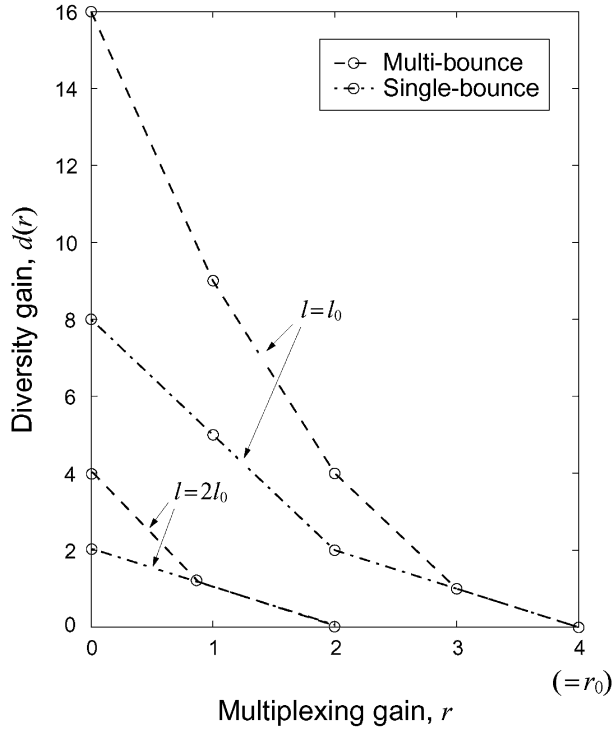

Fig. 10. Illustrates the multiplexing–diversity–range tradeoffs for $M_t = M_r = 2$ at $l = l_0$ and $2l_0$.

are fewer clusters. Now, let us compute the total angle spread. Denote the diameter of the cluster by a and the cluster–cluster separation by b. The distance between the center of the nth cluster to the center of the antenna array is

$$\rho = \sqrt{(n+1/2)^2 b^2 + (l/2)^2}$$

The angle spread due to the nth cluster is

$$\frac{l/2}{\rho} \cdot \frac{a}{\rho} = \frac{la}{2\rho^2}.$$

The total angle spread is therefore given by the sum

$$|\Omega_t| = |\Omega_r| = \frac{4a}{l} \sum_{n=0}^{\infty} \frac{1}{1+(2n+1)^2(b/l)^2}. \tag{49}$$

If $b > a$, it is bounded by

$$\frac{\pi a}{bl}\left(1 - \frac{2}{\pi}\tan^{-1}\frac{b}{l}\right) \le |\Omega_t| = |\Omega_r| \le \frac{\pi a}{bl}\left(1 + \frac{2}{\pi}\tan^{-1}\frac{b}{l}\right) \tag{50}$$

implying

$$|\Omega_t| = |\Omega_r| = \frac{\pi a}{b}\frac{1}{l} + o(1/l) \tag{51}$$

for large l. The total angle spread remains inversely proportional to the propagation range. Suppose $|\Omega_{t0}|$ and $|\Omega_{r0}|$ are the respective transmit and receive angle spread at the reference range $l_0 = 1$ m. We draw the following hypothesis:

$$|\Omega_t| = \frac{|\Omega_{t0}|}{l} \quad \text{and} \quad |\Omega_r| = \frac{|\Omega_{r0}|}{l}. \tag{52}$$

Now, to achieve a propagation range of l, the maximum multiplexing gain would be

$$r_0(l) = \frac{1}{l}\min\{L_t|\Omega_{t0}|, L_r|\Omega_{r0}|\}.$$

One can sacrifice some of the multiplexing gain to obtain a better diversity gain. The tradeoff involved depends on the underlying scattering mechanisms. Fig. 10 gives an example of such tradeoffs among multiplexing gain, diversity gain, and propagation range for the case $r(l_0) = 4$ and $M_t = 2$.

VI. Conclusion

We use the angular intervals subtended by clusters of scatterers to characterize the scattering condition, and study linear arrays that are limited in length but not the number of antennas. Then we model the response within those angular intervals due to basic scattering mechanisms. In the capacity anlysis, we show that for arrays of length L in a physical environment of total angle spread $|\Omega|$, the ergodic capacity increases linearly with $L|\Omega|$ for large arrays. But when antenna arrays reduce to more practical sizes, the number of spatial degrees of freedom depends on the SNR as well. This implies that the number of antennas used would depend on the SNR. In the diversity analysis, we focus on the tradeoff between multiplexing gain (data rate) and diversity gain. Unlike the ergodic capacity, the different scattering mechanisms have distinguishable tradeoffs. These differences would give us more insights into space–time code design. Finally, we attempt to quantify the tradeoff among propagation range, diversity gain, and multiplexing gain which

gives us a more comprehensive perspective on the interplay between possible benefits of multiple-antenna systems.

Appendix I
Proof of Lemma 3.1

First, we solve for μ in (26)

$$\begin{aligned}\mathsf{SNR} &= \int \left(\mu - \frac{1}{x^2}\right)^+ dG(x) + o(\ln(L_t|\Omega_t|)) \\ &= (\mu-1)L_t|\Omega_t| + \frac{1}{\pi^2}M_t \ln(2\pi L_t|\Omega_t|) \\ &\quad \times \left[(\mu-1)\ln(\sqrt{\mu}-1) - \frac{\mu}{2} - \sqrt{\mu} \right. \\ &\qquad \left. + \frac{1}{2(1-\varepsilon)^2} + \frac{1}{1-\varepsilon}\right] \\ &\quad + o(\ln(L_t|\Omega_t|)) \\ &= (\mu-1)L_t|\Omega_t| + o(\ln(L_t|\Omega_t|))\end{aligned}$$

which gives

$$\mu = 1 + \frac{\mathsf{SNR}}{L_t|\Omega_t|} + o(1)$$

as $L_t|\Omega_t| \to \infty$. The capacity can be written as

$$\begin{aligned}C_{SP} &= \int_{1/\sqrt{\mu}}^{1-\varepsilon} \log(x^2\mu)\, dG(x) + o(\ln(L_t|\Omega_t|)) \\ &= \log\mu \int_{1/\sqrt{\mu}}^{1-\varepsilon} dG(x) + 2\int_{1/\sqrt{\mu}}^{1-\varepsilon} \log x\, dG(x) \\ &\quad + o(\ln(L_t|\Omega_t|)).\end{aligned}$$

The first integral is

$$L_t|\Omega_t| + \frac{1}{\pi^2}M_t \ln(2\pi L_t|\Omega_t|)\ln(\sqrt{\mu}-1)$$

and the second integral is

$$\begin{aligned}&\frac{1}{\pi^2 \ln 2} M_t \ln(2\pi L_t|\Omega_t|) \int_{1/\sqrt{\mu}}^{1-\varepsilon} \frac{\ln x}{x} + \frac{\ln x}{1-x}\, dx \\ &\quad = \frac{1}{\pi^2 \ln 2} M_t \ln(2\pi L_t|\Omega_t|) \left[\frac{1}{2}\ln^2(1-\varepsilon) - \frac{1}{8}\ln^2\mu \right. \\ &\qquad \left. + \mathrm{Li}_2(\varepsilon) - \mathrm{Li}_2(1-1/\sqrt{\mu})\right].\end{aligned}$$

As ε tends to 0 when $L_t|\Omega_t|$ tends to ∞, the capacity can be rewritten as

$$\begin{aligned}C_{SP} = [L_t|\Omega_t| + M_t \ln(2\pi L_t|\Omega_t|) f_1(\mathsf{SNR})]\log\mu \\ + o(\ln(L_t|\Omega_t|))\end{aligned}$$

as $L_t|\Omega_t| \to \infty$, where

$$\begin{aligned}f_1(\mathsf{SNR}) &= \frac{1}{\pi^2}\left[\ln(\sqrt{\mu}-1) - \frac{1}{4}\ln\mu \right. \\ &\qquad \left. - \frac{2}{\ln 2}\mathrm{Li}_2(1-1/\sqrt{\mu})/\log\mu\right] \\ &= \frac{1}{4\pi^2}\ln\frac{\mathsf{SNR}}{L_t|\Omega_t|} + o(\ln\mathsf{SNR})\end{aligned}$$

as $\mathsf{SNR} \to \infty$.

Appendix II
Proof of Lemma 3.3

The $F_\epsilon(x)$ can be expressed as

$$\begin{aligned}F_\epsilon(x) = \frac{M_t \ln(2\pi L_t|\Omega_t|)}{\pi^2 \bar{G}(\epsilon)} \left(\ln\frac{1-\epsilon}{\epsilon} - \ln\frac{1-x}{x}\right) \\ + o\left(\frac{\ln(L_t|\Omega_t|)}{L_t|\Omega_t|}\right).\end{aligned}$$

Now, we have

$$\begin{aligned}\int_\epsilon^1 \log x\, dF_\epsilon(x) = -\frac{M_t \ln(2\pi L_t|\Omega_t|)}{2\pi^2 \bar{G}(\epsilon)\ln 2}[\ln^2\epsilon \\ + 2\mathrm{Li}_2(1-\epsilon)] + o\left(\frac{\ln(L_t|\Omega_t|)}{L_t|\Omega_t|}\right)\end{aligned}$$

which yields

$$\begin{aligned}C_{MD} &\gtrsim L_t|\Omega_t| \log\frac{\mathsf{SNR}}{l^{\nu-1}e} + \frac{1}{\pi^2}M_t \ln(2\pi L_t|\Omega_t|) \\ &\quad \times \left[\log\frac{\mathsf{SNR}}{l^{\nu-1}e}\ln\frac{1-\epsilon}{\epsilon} - \log\epsilon\ln\epsilon - \frac{2}{\ln 2}\mathrm{Li}_2(1-\epsilon)\right] \\ &\quad + o(\ln(L_t|\Omega_t|))\end{aligned}$$

as $L_t|\Omega_t| \to \infty$, for all $\epsilon \in (0,1)$. Now, we pick

$$\epsilon = \left(\sqrt{\frac{\mathsf{SNR}}{l^{\nu-1}e}}\right)^{-1} \tag{53}$$

and complete the proof.

Appendix III
Proof of Lemma 3.4

We have

$$\begin{aligned}C_{MD} &\le \int_0^{1-\varepsilon} \log\left(1 + \frac{\mathsf{SNR}}{l^{\nu-1}}x\right) dG(x) + o(\ln(L_t|\Omega_t|)) \\ &= \frac{1}{\pi^2 \ln 2} M_t \ln(2\pi L_t|\Omega_t|) \int_0^{1-\varepsilon} \frac{1}{x}\ln\left(1 + \frac{\mathsf{SNR}}{l^{\nu-1}}x\right) \\ &\quad + \frac{1}{1-x}\ln\left(1 + \frac{\mathsf{SNR}}{l^{\nu-1}}x\right) dx + o(\ln(L_t|\Omega_t|)).\end{aligned}$$

The first integral is

$$-\mathrm{Li}_2\left(-\frac{\mathsf{SNR}}{l^{\nu-1}}(1-\varepsilon)\right)$$

and the second integral is

$$\begin{aligned}&\frac{\pi^2 L_t|\Omega_t|}{M_t \ln(2\pi L_t|\Omega_t|)} \ln\left(1 + \frac{\mathsf{SNR}}{l^{\nu-1}}(1-\varepsilon)\right) \\ &\quad - \ln\left(1 + \frac{\mathsf{SNR}}{l^{\nu-1}}(1-\varepsilon)\right) \ln\frac{\mathsf{SNR}/l^{\nu-1}(1-\varepsilon)}{1 + \mathsf{SNR}/l^{\nu-1}} \\ &\quad - \mathrm{Li}_2\left(\frac{1 + \mathsf{SNR}/l^{\nu-1}(1-\varepsilon)}{1 + \mathsf{SNR}/l^{\nu-1}}\right) \\ &\quad + \mathrm{Li}_2\left(\frac{1}{1 + \mathsf{SNR}/l^{\nu-1}}\right).\end{aligned}$$

As ε approaches 0 for large $L_t|\Omega_t|$ and

$$\lim_{\mathsf{SNR}\to\infty} \frac{-\mathrm{Li}_2(-\mathsf{SNR}/l^{\nu-1})}{\ln^2(\mathsf{SNR}/l^{\nu-1})} = \frac{1}{2}$$

the upper bound can be expressed as

$$C_{MD} \le [L_t|\Omega_t| + M_t \ln(2\pi L_t|\Omega_t|) f_3(\mathsf{SNR})] \times \log\left(1 + \frac{\mathsf{SNR}}{l^{\nu-1}}\right) + o(\ln(L_t|\Omega_t|))$$

as $L_t|\Omega_t| \to \infty$, where

$$f_3(\mathsf{SNR}) = \frac{1}{2\pi^2} \ln \frac{\mathsf{SNR}}{l^{\nu-1}} + o(\ln \mathsf{SNR})$$

as $\mathsf{SNR} \to \infty$.

Appendix IV
Proof of Theorem 4.2

The channel matrix for the single-bounce diffuse channel is block diagonal and each diagonal subblock is an i.i.d. fading channel by itself. Suppose $d_i(r)$ satisfy

$$\lim_{\mathsf{SNR}\to\infty} \frac{\log P[\det(\boldsymbol{I} + \mathsf{SNR}\boldsymbol{H}_i^\dagger \boldsymbol{H}_i) < \mathsf{SNR}^r]}{\log \mathsf{SNR}} = -d_i(r)$$

for $i = 1, \ldots, M_t$. We follow the notation in [15] and use the symbol $\doteq$ to denote

$$\lim_{\mathsf{SNR}\to\infty} \frac{\log g(\mathsf{SNR})}{\log_2 \mathsf{SNR}} = b \iff g(\mathsf{SNR}) \doteq \mathsf{SNR}^b.$$

Then, $d_i(r)$ satisfies

$$P[\det(\boldsymbol{I} + \mathsf{SNR}\boldsymbol{H}_i^\dagger \boldsymbol{H}_i) < \mathsf{SNR}^r] \doteq \mathsf{SNR}^{-d_i(r)}.$$

Let $\mathsf{SNR}^{\theta_i} = \det(\boldsymbol{I} + \mathsf{SNR}\boldsymbol{H}_i^\dagger \boldsymbol{H}_i)$. The cumulative distribution function (cdf) of θ_i is

$$F_{\theta_i}(\theta) = P(\theta_i < \theta) \doteq \mathsf{SNR}^{-d_i(\theta)}$$

and thus, its probability density function (pdf) is

$$\begin{aligned} f_{\theta_i}(\theta) &\doteq \frac{d}{d\theta} \mathsf{SNR}^{-d_i(\theta)} \\ &= \mathsf{SNR}^{-d_i(\theta)} \ln \mathsf{SNR} \frac{d}{d\theta} d_i(\theta) \\ &\doteq \mathsf{SNR}^{-d_i(\theta)} \end{aligned}$$

ignoring the sign. Since the subblocks are independent, so

$$\begin{aligned} &P\left[\prod_{i=1}^{M_t} \det(\boldsymbol{I} + \mathsf{SNR}\boldsymbol{H}_i^\dagger \boldsymbol{H}_i) < \mathsf{SNR}^r\right] \\ &= P\left(\sum_{i=1}^{M_t} \theta_i < r\right) \\ &= (F_{\theta_1} * f_{\theta_2} * \cdots * f_{\theta_{M_t}})(r) \\ &\doteq \mathsf{SNR}^{-d_{SD}(r)} \end{aligned}$$

where

$$d_{SD}(r) = (d_1 \oplus d_2 \oplus \cdots \oplus d_{M_t})(r).$$

Now, we will show that $d_{SD}(r)$ is obtained by putting end-to-end the different linear pieces in $d_i(r)$'s, sorted by increasing slopes (or, equivalently, decreasing negative slopes). It is sufficient to show that it holds for $M_t = 2$. Let $\tilde{d}(r)$ denote the claimed curve, and the slopes of $d_1(r)$ and $d_2(r)$ be $0 \ge s_1 \ge s_2 \ge \cdots \ge s_L$, with the corresponding length of projection onto the horizontal axis being $\alpha_1, \alpha_2, \cdots, \alpha_L$ where

$$L = \min\{L_t|\Omega_{t,1}|, L_r|\Omega_{r,1}|\} + \min\{L_t|\Omega_{t,2}|, L_r|\Omega_{r,2}|\}.$$

Furthermore, let $\mathcal{S}_n$ be the set of index of slopes belonging to $d_n(r)$, for $n = 1, 2$. Then, for $r \in [L - \sum_{i=1}^{l} \alpha_i, L - \sum_{i=1}^{l-1} \alpha_i]$, the claimed curve is given by

$$\tilde{d}(r) = -\sum_{i=1}^{l-1} s_i \alpha_i - s_l \left(L - \sum_{i=1}^{l-1} \alpha_i - r\right).$$

Assume, without loss of generality, $l \in \mathcal{S}_2$. We will show that when $r = L - \sum_{i=1}^{l-1} \alpha_i - \Delta$ for some $\Delta \in [0, \alpha_l)$

$$d_1(u) + d_2(r-u) \ge d_1(a) + d_2(b), \qquad \forall u \in [0, r]$$

where

$$\begin{aligned} a &= \min\{L_t|\Omega_{t,1}|, L_r|\Omega_{r,1}|\} - \sum_{\substack{1 \le i \le l-1 \\ i \in \mathcal{S}_1}} \alpha_i \\ b &= \min\{L_t|\Omega_{t,2}|, L_r|\Omega_{r,2}|\} - \sum_{\substack{1 \le i \le l-1 \\ i \in \mathcal{S}_2}} \alpha_i - \Delta. \end{aligned}$$

As $d_n(r)$'s are decreasing and piecewise linear, when $u \le a$

$$d_1(u) - d_1(a) \ge -s_l(a-u).$$

Note that $a + b = r$ and, hence, $r - u \ge b$. Thus,

$$d_2(b) - d_2(r-u) \le -s_l(r-u-b) = -s_l(a-u).$$

Combining both inequalities gives the desired result. Similarly, when $u > a$

$$\begin{aligned} d_1(a) - d_1(u) &\le -s_l(u-a) \\ d_2(r-u) - d_2(b) &\ge -s_l(b-r+u) = -s_l(u-a). \end{aligned}$$

Combining them gives the desired result as well. Furthermore, we have

$$\begin{aligned} d_1(a) + d_2(b) &= -\sum_{\substack{1 \le i \le l-1 \\ i \in \mathcal{S}_1}} s_i \alpha_i - \sum_{\substack{1 \le i \le l-1 \\ i \in \mathcal{S}_2}} s_i \alpha_i - s_l \Delta \\ &= -\sum_{i=1}^{l-1} s_i \alpha_i - s_l \left(L - \sum_{i=1}^{l-1} \alpha_i - r\right) \\ &= \tilde{d}(r). \end{aligned}$$

This implies that $d_1(u) + d2(r-u) \ge \tilde{d}(r)$. Since $d_{SD}(r)$ is the infimum of the sum on the left over all u from 0 to r, it must coincide with the claimed curve on the right.

References

[1] D. S. Shiu, G. J. Foschini, M. J. Gans, and J. M. Kahn, "Fading correlation and its effect on the capacity of multielement antenna systems," *IEEE Trans. Commun.*, vol. 48, no. 3, pp. 502–513, Mar. 2000.

[2] H. Bölcskei, D. Gesbert, and A. J. Paulraj, "On the capacity of OFDM-based spatial multiplexing systems," *IEEE Trans. Commun.*, vol. 50, no. 2, pp. 225–234, Feb. 2002.

[3] C. N. Chuah, D. Tse, J. M. Kahn, and R. A. Valenzuela, "Capacity scaling in MIMO wireless systems under correlated fading," *IEEE Trans. Inf. Theory*, vol. 48, no. 3, pp. 637–650, Mar. 2002.

[4] D. Gesbert, T. Ekman, and N. Christophersen, "Capacity limits of dense palm-sized MIMO arrays," in *Proc. IEEE Global Telecommun. Conf.*, vol. 2, Taipei, Taiwan, Nov. 2002, pp. 17–21.

[5] J. Salz and J. H. Winters, "Effect of fading correlation on adaptive arrays in digital mobile radio," *IEEE Trans. Veh. Technol.*, vol. 43, no. 4, pp. 1049–1057, Nov. 1994.

[6] G. G. Raleigh and J. M. Cioffi, "Spatio-temporal coding for wireless communication," *IEEE Trans. Commun.*, vol. 46, no. 3, pp. 357–366, Mar. 1998.
[7] A. M. Sayeed, "Deconstructing multi-antenna fading channels," *IEEE Trans. Signal Processing*, vol. 50, no. 10, pp. 2563–2579, Oct. 2002.
[8] T. S. Pollock, T. D. Abhayapala, and R. A. Kennedy, "Antenna saturation effects on MIMO capacity," in *Proc. IEEE Int. Conf. Communications*, vol. 3, Anchorage, AK, May 2003, pp. 2301–2305.
[9] M. Debbah and R. Müller, "MIMO channel modeling and the principle of maximum entropy," in *IEEE Trans. Inf. Theory*, vol. 51, May 2005, pp. 1667–1690.
[10] R. R. Müller, "A random matrix model of communication via antenna arrays," *IEEE Trans. Inf. Theory*, vol. 48, no. 9, pp. 2495–2406, Sep. 2002.
[11] A. S. Y. Poon, R. W. Brodersen, and D. N. C. Tse, "Degrees of freedom in multiple-antenna channels: A signal space approach," *IEEE Trans. Inf. Theory*, vol. 51, no. 2, pp. 523–536, Feb. 2005.
[12] J. W. Wallace and M. A. Jensen, "Intrinsic capacity of the MIMO wireless channel," in *Proc. IEEE Veicular Technology Conf.*, vol. 2, Vancouver, BC, Canada, Sep. 2002, pp. 701–705.
[13] T. S. Rappaport, *Wireless Communications: Principle and Practice*, 2nd ed. Upper Saddle River, NJ: Prentice-Hall, 2002.
[14] H. Özcelik, M. Herdin, W. Weichselberger, J. Wallace, and E. Bonek, "Deficiencies of Kronecker MIMO radio channel model," *Electron. Lett.*, vol. 39, no. 16, pp. 1209–1210, Aug. 2003.
[15] L. Zheng and D. N. C. Tse, "Diversity and multiplexing: A fundamental tradeoff in multiple antenna channels," *IEEE Trans. Inf. Theory*, vol. 49, no. 5, pp. 1073–1096, May 2003.
[16] I. J. Gupta and A. A. Ksienski, "Effect of mutual coupling on the performance of adaptive arrays," *IEEE Trans. Antennas Propag.*, vol. AP-31, no. 5, pp. 785–791, Sep. 1983.
[17] N. J. Kirsch and K. R. Dandekar, "Modeling effects of mutual coupling considered at both ends of a MIMO channel using computational electromagnetics," in *Proc. IEEE Veicular Technology Conf.*, vol. 6, Los Angeles, CA, 2004, pp. 4352–4355.
[18] D. F. Kelley and W. L. Stutzman, "Array antenna pattern modeling methods that include mutual coupling effects," *IEEE Trans. Antennas Propag.*, vol. 41, no. 12, pp. 1625–1632, Dec. 1993.
[19] T. Su and H. Ling, "On modeling mutual coupling in antenna arrays using the coupling matrix," *Microw. Opt. Technol. Lett.*, vol. 28, no. 4, pp. 231–237, Feb. 2001.
[20] L. Tsang, J. A. Kong, and K. H. Ding, *Scattering of Electromagnetic Waves: Theories and Applications*. New York: Wiley, 2000.
[21] H. J. Landau and H. Widom, "Eigenvalue distribution of time and frequency limiting," *J. Math. Anal. Applic.*, vol. 77, pp. 469–481, 1980.
[22] D. Slepian, "Some asymptotic expansions for prolate spheroidal wave functions," *J. Math. and Phys.*, vol. 44, pp. 99–140, 1965.
[23] R. G. Gallager, *Information Theory and Reliable Communication*. New York: Wiley, 1968.
[24] V. L. Girko, *Theory of Random Determinants*. Norwell, MA: Kluwer, 1990.
[25] A. L. Moustakas, S. H. Simom, and A. M. Sengupta, "MIMO capacity through correlated channels in the presence of correlated interferers and noise: A (not so) large N analysis," *IEEE Trans. Inf. Theory*, vol. 49, no. 10, pp. 2545–2561, Oct. 2003.
[26] A. M. Tulino, A. Lozano, and S. Verdú, "Impact of antenna correlation on the capacity of multiantenna channels," *IEEE Trans. Inf. Theory*, vol. 51, no. 7, pp. 2491–2509, Jul. 2005.
[27] D. Gesbert, "Multipath: Curse or blessing? A system performance analysis of MIMO wireless systems," in *Proc. Int. Zurich Seminar on Communications*, Zurich, Switzerland, 2004, pp. 14–17.
[28] J. L. Harris, "Diffraction and resolving power," *J. Opt. Soc. Amer.*, vol. 54, no. 7, pp. 931–936, Jul. 1964.
[29] G. T. di Francia, "Resolving power and information," *J. Opt. Soc. Amer.*, vol. 45, no. 7, pp. 497–501, Jul. 1955.
[30] D. N. C. Tse and P. Viswanath, *Fundamentals of Wireless Communication*. Cambridge, U.K.: Cambridge Univ. Press, 2005.
[31] Ö. Oyman, R. U. Nabar, H. Bölcskei, and A. J. Paulraj, "Characterizing the statistical properties of mutual information in MIMO channels," *IEEE Trans. Signal Process.*, vol. 51, no. 11, pp. 2784–2795, Nov. 2003.